Hindawi
Journal of Chemistry
Volume 2018, Article ID 9585728, 7 pages
https://doi.org/10.1155/2018/9585728

Research Article

Investigation on Smoke Suppression Mechanism of Hydrated Lime in Asphalt Combustion

Kai Zhu,[1,2] **Yunhe Wang**,[1] **Qi Zhou**,[3] **Daquan Tang**,[1] **Lingzhu Gu**,[4,5] **and Ke Wu**[4,6]

[1]*College of Quality and Safety Engineering, China Jiliang University, Hangzhou 310018, China*
[2]*Ningbo Communication Engineering Construction Group Co., Ltd., Ningbo 315099, China*
[3]*Wenzhou Traffic Quality Supervision Bureau, Wenzhou 325000, China*
[4]*College of Civil Engineering and Architecture, Zhejiang University, Hangzhou 310058, China*
[5]*Department of Civil and Environmental Engineering, University of Illinois at Urbana-Champaign, 205 N Mathews Ave., MC-250, Urbana, IL 61801, USA*
[6]*Key Laboratory of Offshore Geotechnics and Material of Zhejiang Province, Zhejiang University, Hangzhou 310058, China*

Correspondence should be addressed to Ke Wu; wuke@zju.edu.cn

Received 26 May 2018; Accepted 29 August 2018; Published 26 September 2018

Academic Editor: Ewa Schab-Balcerzak

In this study, cone calorimeter and thermogravimetric analyses were used to simulate the asphalt combustion process under the conditions of fire radiation and programmed temperature increase. The gaseous compositions and release rules were analyzed by infrared spectroscopy to investigate the influence of hydrated lime on the smoke suppression mechanism in the asphalt combustion process. The experimental results show that hydrated lime can promote the asphalt mastic surface to form a barrier layer during the combustion process. This barrier layer can reduce the burning intensity of asphalt. Although the compositions of gaseous products do not change much, the rates of CO production and smoke release are decreased. In addition, hydrated lime is alkaline and can thus neutralize acidic gases such as SO_2 and reduce the toxicity of gaseous products. With the addition of 40 wt.% hydrated lime, the total smoke release and the CO release rate both decrease by more than 20% relative to the addition of the same amount of limestone fillers and decrease by more than 10% relative to the addition of the same amount of magnesium hydroxide flame retardant.

1. Introduction

Asphalt is a combustible mixture composed of hydrocarbons and relatively nonmetallic derivatives, which is wildly used in road pavement and waterproofing systems [1, 2]. The combustion of asphalt is typically accompanied with a quantity of toxic smoke [3, 4], seriously endangering any personnel within the affected areas. To solve this problem, applying flame retardant to asphalt has become a common way to reduce the hazards associated with pavement during tunnel fires [5–12].

Due to their nontoxic characteristics and their capability for smoke suppression, metal hydroxides are prevalently used to modify the flame resistance of asphalt [7–12]. Among them, hydrated lime did not initially attract the attention of researchers since it decomposes at a relatively high temperature that exceeds the ignition point of asphalt [13]. However, some recent studies have shown different results. Hydrated lime has been proved to promote the formation of a dense inert layer on the asphalt surface by carbonation in the combustion process [7], thus inhibiting the continuous combustion of asphalt, serving as an excellent flame retardant [14]. However, the mechanism of how hydrated lime affects the smoke release of asphalt during combustion requires further study.

The smoke release characteristics of asphalt during combustion have been investigated by the combination of a simulated combustion test platform and smoke analyzer. Wu et al. [4] studied the smoke release law of asphalt and binder at a high rate of heating by combining a fixed bed

combustion test and infrared spectroscopy. It was observed that the main gaseous products from asphalt combustion include CO_2, CO, NO, NO_2, and SO_2, and that the volatile components of asphalt are the key factors influencing the smoke release rate (RSR) during combustion. Puente et al. [15] studied the combustion characteristics of an asphalt mixture at a radiation intensity of $50\,kW{\cdot}m^{-2}$ by the combination method of cone calorimeter-Fourier transform infrared spectroscopy (FTIR) and analyzed the release characteristics of CO_2, CO, and SO_2 in combustion. Additionally, Xu and Huang [11, 12] analyzed the combustion procedure of asphalt binder during the process of temperature rise by thermogravimetric analysis (TGA)- FTIR, revealing the mechanism of how $Mg(OH)_2$ affects the release of gaseous products during the various reaction stages of asphalt. In addition, by TGA-MS (mass spectrometry) analysis, Zhao et al. [16] investigated the components and release characteristics of smoke produced from the combustion of four components of asphalt. These studies indicate that combustion test methods [4, 15], especially the fixed bed combustion test and cone calorimeter, can be used to simulate the actual burning environment with a high rate of temperature rise and strong radiation, but it is challenging to analyze the specific reaction process accurately. Temperature-programmed combustion test methods [11, 12, 16], such as TGA, are more effective in analyzing the different smoke release characteristics and mechanisms of asphalt combustion during each reaction temperature range, but the reaction condition is quite different from the real situation. A comparison between these two methods is still lacking in the research conducted to date.

This paper explores how hydrated lime influences the toxic smoke release during asphalt combustion by cone calorimeter analyses; it also explains the mechanism of smoke suppression by hydrated lime via TGA-FTIR, providing a more complete understanding of the smoke suppression characteristics of hydrated lime.

2. Experimental

2.1. Materials. The asphalt used in the test, SK70, was obtained from Bao Li Asphalt Co., Ltd. in Jiangsu province, China, with 63.8×0.1 mm penetration at 25°C, ductility of 42 cm at 10°C, and a softening point of 47.9°C. The rotational viscosity of the asphalt is 193 Pa·s at 60°C, while the flash point is 340°C, and the ignition point is 375°C. The components, proximate, and ultimate analyses of the sample are shown in Table 1.

The mineral fillers used included $Ca(OH)_2$ (the main component of hydrated lime), $CaCO_3$ (the main component of limestone), and $Mg(OH)_2$, all of which were of analytical reagent grade and provided by Aladdin Chemical Co., Ltd. The corresponding pH values were 12, 9, and 10.

The procedure of binder preparation was as follows. The asphalt binder was initially heated to 160 ± 5°C. Then, the asphalt was stirred by a BME100LT-N dispersion machine, and 40 wt.% $Ca(OH)_2$, $CaCO_3$, or $Mg(OH)_2$ was added gradually. A BME100LT high-shear hybrid emulsifier was used to stir for another 30 min at a speed of $5000\,r{\cdot}min^{-1}$ to ensure the uniform distribution of additive in the asphalt binder. Then, the mixture was stirred for 15 min more at a speed of $500\,r{\cdot}min^{-1}$ to eliminate air bubbles. Finally, the heating was stopped, and stirring was continued until the binder cooled down.

2.2. Test Methods. A cone calorimeter (FFT 007 type) was adopted to measure the smoke release parameters of the asphalt binder according to the ISO-5660 standard. The sample was poured into a round cake shape with an inner diameter of 70 mm and a thickness of 10 mm. The sample was covered with aluminum foil at the side and bottom, and with insulated cotton at the bottom to reduce the environmental influence. The radiation intensity selected in this study was $50\,kW{\cdot}m^{-2}$ (higher than the critical radiation of the asphalt mixture, $30\,kW{\cdot}m^{-2}$ [17]), representing the thermal radiation levels of a medium-sized fire [18], and the specimen surface temperature was approximately 610°C. The CO concentration and smoke concentration were measured by a nondispersive infrared spectroscopy (NDIR) gas sensor and helium-neon laser photoemission measurement system, respectively. The experiments were conducted three times under each condition, and the average values were calculated.

The process of material weight loss during a temperature rise was simulated by thermogravimetry. The smoke release situation during the heating process was analyzed by a Fourier-transform infrared spectrometer (Nexus670) and a thermogravimetric analyzer (TGA/SDTA851e). Approximately 10 mg of the sample was placed in an Al_2O_3 crucible, which was heated from 50°C to 850°C at a rate of $10°C\,min^{-1}$ and then reacted at a constant temperature for 15 min. The gas-injected TG test system was composed of 21% oxygen and 79% nitrogen by volume. Considering the sensitivity of infrared detection and the possibility of escaping gas return, the carrier flow rate was set to $90\,mL{\cdot}min^{-1}$. The resolution of the Fourier-infrared spectrometer was $4\,cm^{-1}$, and the scan frequency was 20 times per minute.

A FEI Quanta FEG 650 field emission scanning electron microscope (SEM) was used to obtain SEM images of the combustion residues.

3. Results and Discussion

3.1. Cone Calorimeter Analysis. The cone calorimeter test was performed on the base binder (BA), 40 wt.% hydrated lime modified binder (HL), 40 wt.% limestone modified binder (LS), and 40 wt.% magnesium hydroxide modified binder (MH), simulating the asphalt combustion process under a fire condition with $50\,kW{\cdot}m^{-2}$ radiation intensity. The heat release features were reported in our previous paper [7]; the test results of the smoke release characteristics are shown in Table 2.

The average RSR of HL was $10.32\,m^2{\cdot}m^{-2}{\cdot}s^{-1}$, a decrease of 36.5% relative to BA and 24.5% relative to LS. These results suggest that in addition to serving as a filler, hydrated lime also provides a smoke suppression effect. Moreover, the RSR of HL is 3.2% lower than that of the binder modified with the traditional flame retardant, MH.

Table 1: Components, proximate, and ultimate analyses of the sample.

Components analysis/wt.%				Proximate analysis/wt.%, ad				Ultimate analysis/wt.%, ad				
Sa	Ar	Re	As	M	A	V	FC	C	H	N	S	O
21.1	50.2	20.7	7.9	1.7	0.6	83.9	13.8	84.4	10.9	0.5	2.7	0.9

Sa: saturates; Ar: aromatics; Re: resin; As: asphaltenes; ad: air-dried basis; M: moisture; A: ash; V: volatile; FC: fixed carbon.

Table 2: Smoke release properties obtained from cone calorimeter.

Samples	RSR ($m^2 \cdot m^{-2} \cdot s^{-1}$)	TSR ($m^2 \cdot m^{-2}$)	TTI (s)	RYR (%)	COR (%)	COY ($kg \cdot kg^{-1}$)
BA	16.25	15319	25	14.4	0.0186	0.0729
HL	10.32	9383	60	39.7	0.0083	0.0571
LS	13.67	13187	49	28.4	0.0115	0.0728
MH	10.66	11309	70	35.9	0.0107	0.0641

RSR: rate of smoke release; TSR: total smoke release; TTI: time to ignition; RYR: residue yield ratio; COR: carbon monoxide ratio; COY: carbon monoxide yield.

Figure 1 further compares the RSR of BA with the three modified binders, that is, HL, LS, and MH, over time. Under the thermal radiation, BA is first ignited at 25 s, and the release rate of the smoke increases rapidly. Due to the addition of mineral filler, the ignition time of the three modified binders is longer compared with that of BA, and the RSR is significantly slower than that of BA. A comparison of the smoke release curves of the three modified binders indicates that the increasing rate of the RSR of LS is the fastest, while that of MH is the slowest, and that of HL is the intermediate. Although HL has a higher RSR at the initial combustion stage than MH, this rate steadily declines after reaching the early peak. Moreover, the RSR of MH continues to rise, gradually surpassing HL, and reaches the peak at approximately 545 s. The reason for the difference between the two smoke release characteristics is explained as follows. During the combustion of MH, the strength of the residue produced is lower, which serves as the barrier layer of combustion. This layer tends to fail at the later stage of combustion, however, causing the combustion to intensify; thus, the rate of smoke release continues to increase. However, in the combustion of HL, $CaCO_3$ generated through the carbonation of hydrated lime promotes the formation of an inert dense layer on the asphalt surface [7], retarding the combustion and suppressing the smoke. Hence, the RSR declines faster. This result indicates that the inert barrier layer plays an important role in the smoke suppression process, which can effectively insulate the heat transfer between asphalt and the external environment, thus reducing the RSR of asphalt combustion.

The total smoke release volume (TSR) of HL is 9383 $m^2 \cdot m^{-2}$, which is not only 28.8% lower than that of LS (13187 $m^2 \cdot m^{-2}$) but also 17.0% lower than that of MH. Therefore, it can be concluded that the total RSR decreases more than the average RSR because of the increase in the residue yield ratio (RYR) of asphalt during combustion due to the barrier layer of the hydrated lime.

CO is a product of the incomplete combustion of asphalt and is a deadly factor in tunnel fires. Figure 2 shows the CO concentrations of BA and three modified binders during the combustion process. Associated with the smoke release condition in Figure 1, the CO concentration curve corresponds to the variation trend of the smoke release curve, and all the CO concentrations of the three modified binders are significantly lower than that of BA. In terms of the numerical value, the average CO concentration of HL decreases by 55.5% relative to that of BA, much larger than the decrease in smoke release (36.5%), probably because the filler is scattered by fire plumes during combustion and thus becomes part of the smoke, while the release of CO is not affected by this mechanism.

The carbon monoxide production yield (COY) represents the CO mass produced by the combustion of the asphalt with unit mass, describing the ratio of the CO generated from incomplete combustion. As Table 2 shows, there is no significant decline in the COY of LS relative to BA, indicating that the decrease in CO concentration mentioned above is caused by the lower combustion rate. However, the COY of HL shows a 21.7% decrease relative to BA and shows a 10.9% decrease relative to MH.

3.2. TGA-FTIR Analysis. Based on the fundamental conclusion obtained from the cone calorimeter analysis that hydrated lime can inhibit the combustion of asphalt binder, this section further analyzes the smoke suppression effect of hydrated lime at each combustion stage of asphalt binder by the TGA-FTIR test. Figure 3 compares the process of mass loss of BA and 40 wt.% hydrated lime modified binder (HL) during the temperature rise.

Figure 4 indicates that there are three major stages during the weight loss process of HL, while BA has only two stages. For both BA and HL, the peak of the derivative weight loss (DTG) curve of the first and second stages appears at temperatures of approximately 460°C and 600°C, respectively; thus, these temperatures are selected as the feature temperatures in infrared spectroscopy analysis. Moreover, the peak of the DTG curve, 760°C, is taken to correspond to the third combustion stage of HL. The relative spectra are shown in Figures 5–7.

Figure 5 shows the spectra of the gaseous products in the first stage of asphalt combustion, which exhibit several transmittance peaks. Through spectroscopy retrieval, it is observed that for both BA and HL, the smoke is a complex mixture composed of various inorganic and organic

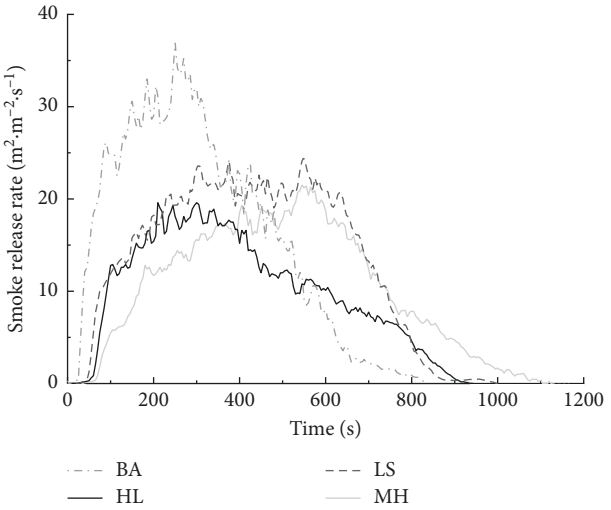

Figure 1: RSR curves of asphalt binder and mastics.

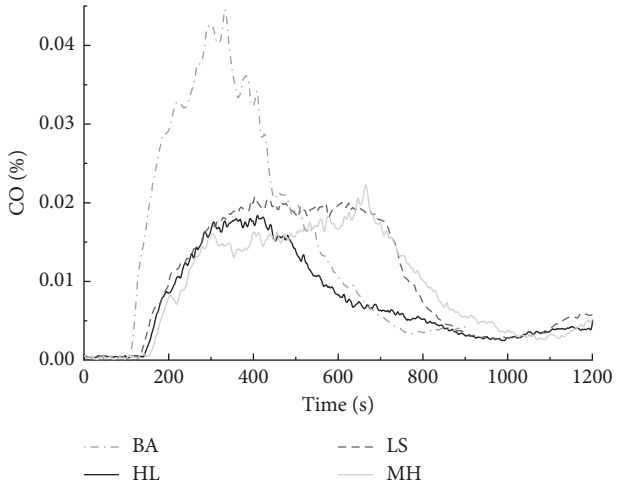

Figure 2: CO fraction curves of asphalt binder and mastics.

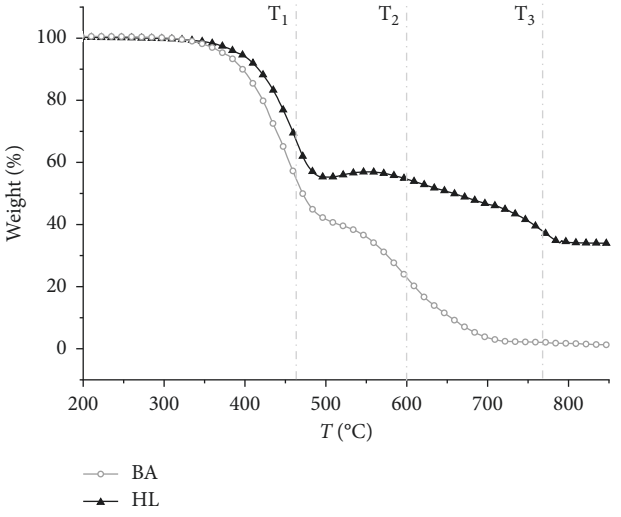

Figure 3: Weight loss curves of BA and HL.

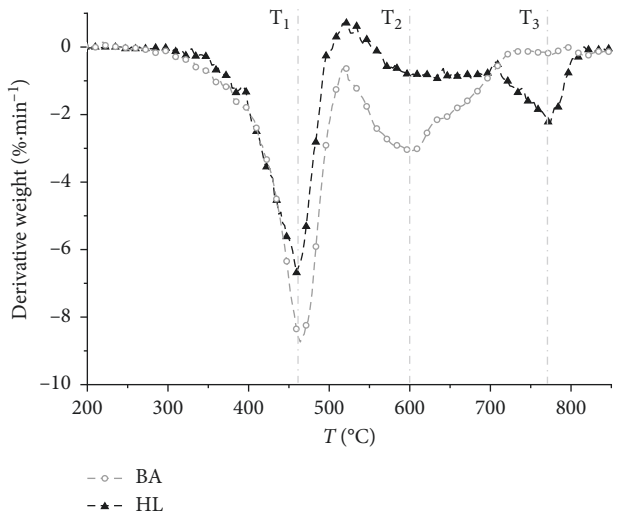

Figure 4: Derivative weight loss curves of BA and HL.

volatiles. Comparing the two spectra, the same peak position is found, which suggests that with the addition of hydrated lime, there is no significant change in the gaseous products during combustion.

In Figure 5, the strongest peaks can be observed at the bands of 2400–2230 cm^{-1} and 790–630 cm^{-1} for both the infrared spectra of BA and HL, which is caused mainly by the generation of CO_2. CO_2 is produced from the complete combustion of organic components in asphalt, and the fracture and reforming of carboxyl (-COOH) and carbonyl groups (C=O).

The two bands at 2200–2050 cm^{-1} are characteristic peaks of CO. Relative to BA, the magnitude of CO twin peaks of the asphalt binder modified by hydrated lime is significantly lower, suggesting that the addition of hydrated lime effectively inhibits the release of CO, which is consistent with the results obtained from the cone calorimeter analysis in Section 3.1.

The bands appearing at 4000–3400 cm^{-1}, 2100–1200 cm^{-1}, and 600–400 cm^{-1} correspond to H_2O. As shown in Figure 5, the magnitude of the transmittance peak of HL from 2100 to 1200 cm^{-1} is larger than that of BA, resulting from the decomposition reaction of $Ca(OH)_2$ in hydrated lime modified binder in the first stage of asphalt combustion, which generates water. Water dilutes the flammable gas concentration to a certain extent, thus inhibiting combustion and smoke generation.

The band at 1400–1300 cm^{-1} corresponds mainly to the stretching vibration of S=O [19], caused by the SO_2 generated from the combustion of sulfur components in asphalt, while the bands at 1630–1550 cm^{-1} and 1950–1750 cm^{-1} may be related to the generation of NO_2 and NO. In this stage, the combustion reaction temperature is relatively low, and the generated nitrogen oxides are mainly of fuel type [20], which means that NO_x is produced from the oxidation of nitrogen in asphalt. The ultimate analysis (Table 1) shows that the nitrogen content in the asphalt is low; thus, both of the NO_x transmittance peaks in the combustion of BA and HL are weak.

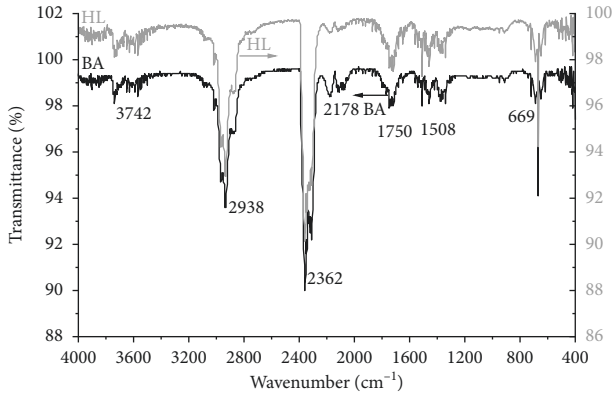

Figure 5: Infrared spectra of gaseous volatiles in the first combustion stage of BA and HL.

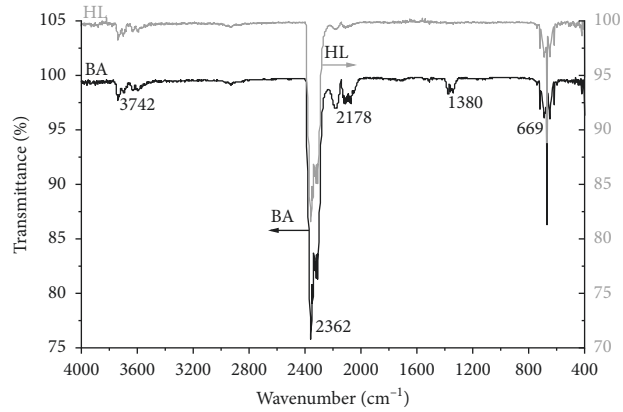

Figure 6: Infrared spectra of gaseous volatiles in the second combustion stage of BA and HL.

In addition, intense bands appear at 3050–2800 cm^{-1} for both BA and HL. These bands likely arise due to the pyrolysis of the light oil components in asphalt (saturates and aromatics) and resin, resulting in a quantity of aliphatic and aromatic compounds. Furthermore, the band at 2900 cm^{-1} is assigned to the stretching vibration of C–H in CH_2 or CH_3, which indicates the generation of benzene or phenol compounds with hydrocarbons as substituents. The bands at approximately 3000 cm^{-1} indicate the formation of methyl due to the decomposition of aliphatic hydrocarbon and aromatic alkyl side chain in asphalt combustion [21]. Moreover, the band at 3030 cm^{-1} is possibly the transmittance of the stretching vibration of C–H in unsaturated polycyclic aromatic hydrocarbons. In addition, transmittance bands appear at approximately 2820 cm^{-1} and 1720 cm^{-1}, which are attributed mainly to the vibration of C–H and C=O, respectively, representing the production of formaldehyde, acetaldehyde, and other aldehydes.

Furthermore, the bands at 770–630 cm^{-1} correspond to the characteristic peaks of aromatic compounds, indicating the separation of aromatic compounds. Figure 5 indicates that the magnitude of the transmittance peak of HL is lower than that of BA. Since aromatic compounds are one of the important precursors of the smoke in asphalt combustion, this finding also explains the antismoking effect of hydrated lime in the cone calorimeter test.

Figure 6 shows the infrared spectroscopy of the gaseous products in the second stage of asphalt combustion. Relative to the first stage, there are fewer types of gaseous products, including CO_2, CO, H_2O, SO_2, and other inorganic gaseous products. Moreover, neither BA nor HL shows significant organic gas absorption bands at approximately 3050–2800 cm^{-1}.

In addition, the magnitude of the CO_2 transmittance peak in the second stage of asphalt combustion is significantly more intense than that in the first stage, increasing from 10% to 25%, indicating that the CO_2 release rate of the second stage is considerably increasing. This result can be explained by the generation of a large amount of combustible organic gas from the pyrolysis of the light components of asphalt in the first stage of combustion. Moreover, in the second stage, the heavy components of asphalt combust, generating combustion products include CO_2, H_2O, SO_2, and CO.

A comparison of the differences in gaseous products before and after the addition of hydrated lime in the second stage of asphalt combustion in Figure 6 indicates that the peak values of the transmittance peaks of HL combustion products are weaker than that of BA, especially the peak height of CO, which decreases by more than 50%. The reason is that with the addition of hydrated lime, a barrier layer is formed during asphalt combustion. The combustion residue SEM images of BA and HL are shown in Figure 7. The barrier layer of HL shows fewer pores in the surface than that of BA, thus reducing the amount of asphalt participating in the combustion and the intensity of the reaction. With a weaker reaction intensity, the generation rate of CO is reduced.

Additionally, due to its high alkalinity, hydrated lime can effectively neutralize the acid toxic gases released from asphalt combustion, e.g., SO_2. Therefore, the FTIR spectrum of BA shows significant characteristic peaks of SO_2 at approximately 1400–1300 cm^{-1}, whereas the corresponding peaks never appear in the spectrum of HL. It can be concluded that hydrated lime has a significant effect on reducing the toxicity of the smoke from asphalt combustion.

Figure 8 shows the gaseous products in the third stage of HL combustion, which do not exist for BA. The major product in this stage is CO_2, generated from (1) the decomposition products of $CaCO_3$ produced by the carbonation of $Ca(OH)_2$ and (2) the combustion product of the barrier-coated asphalt. This process is consistent with the explanation of the mechanism that $CaCO_3$ obtained from the carbonation of $Ca(OH)_2$ promotes the formation of a dense inert layer on the surface of asphalt.

4. Conclusions

(1) With the addition of 40 wt.% of hydrated lime, the total smoke release and the CO release rate are both decreased by more than 20% relative to the addition of the same amount of limestone fillers and are decreased by more than 10% relative to the addition of the same amount of magnesium hydroxide flame retardant.

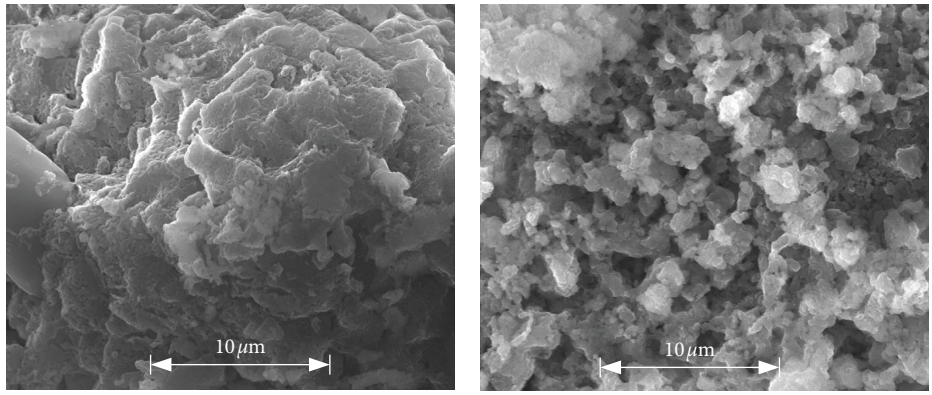

(a) (b)

Figure 7: Combustion residue SEM images of (a) HL and (b) BA.

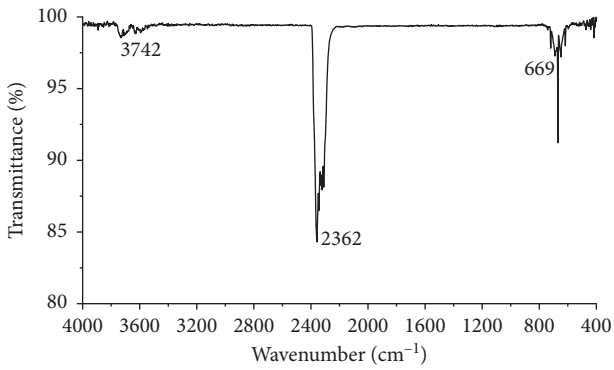

Figure 8: Infrared spectra of gaseous volatiles in the third combustion stage of HL.

(2) With the addition of hydrated lime, there is no prominent difference in the type of gaseous products released during the two stages of asphalt combustion, whereas the relative contents of CO and SO_2 are decreased.

(3) The dense barrier layer formed by the reaction of hydrated lime in the asphalt combustion process can effectively inhibit the reaction intensity of asphalt combustion, thus reducing the CO yield and smoke emission.

(4) Hydrated lime has a strong alkalinity, which can neutralize the acidic gases such as SO_2 and reduce the smoke toxicity.

Data Availability

The data used to support the findings of this study are included within the article.

Additional Points

(i) Hydrated lime can contribute to a barrier layer and suppress the smoke emission. (ii) Hydrated lime effectively suppresses the CO release during asphalt combustion. (iii) Hydrated lime can absorb sulfur dioxide from asphalt combustion. (iv) The influence of hydrated lime on volatiles release was investigated.

Conflicts of Interest

The authors declare that they have no conflicts of interest.

Acknowledgments

This work was funded by the Zhejiang Provincial Natural Science Foundation (No. LQ17E080011), the Key Research and Development Project of Zhejiang Province (No. 2018C03029), the National Natural Science Foundation of China (Nos. 51808521 and 51408542), and Postdoctoral Foundation by Zhejiang Province of China (No. 2017-44).

References

[1] J. Yu, P. Cong, and S. Wu, "Investigation of the properties of asphalt and its mixtures containing flame retardant modifier," *Construction and Building Materials*, vol. 23, no. 6, pp. 2277–2282, 2009.

[2] L. Fan, L. Wong, and G. Ma, "Experimental investigation and modeling of viscoelastic behavior of concrete," *Construction and Building Materials*, vol. 48, pp. 814–821, 2013.

[3] H. Shi, T. Xu, and R. Jiang, "Combustion mechanism of four components separated from asphalt binder," *Fuel*, vol. 192, pp. 18–26, 2017.

[4] K. Wu, K. Zhu, Z. Huang, J. Wang, Q. Yang, and P. Liang, "Research on the combustion mechanism of asphalt and the composition of harmful gas based on infrared spectral analysis," *Spectroscopy and Spectral Analysis*, vol. 32, no. 8, pp. 2089–2094, 2012.

[5] X. Qin, S. Zhu, S. Chen, and K. Deng, "The mechanism of flame and smoke retardancy of asphalt mortar containing composite flame retardant material," *Construction and Building Materials*, vol. 41, pp. 852–856, 2013.

[6] B. Li, Y. Wen, and X. Li, "Laboratory evaluation of pavement performance and burning behavior of flame-retardant asphalt mixtures," *Journal of Testing and Evaluation*, vol. 45, no. 1, pp. 9–17, 2017.

[7] K. Wu, K. Zhu, C. Kang, B. Wu, and Z. Huang, "An experimental investigation of flame retardant mechanism of

hydrated lime in asphalt mastics," *Materials and Design*, vol. 103, pp. 223–229, 2016.

[8] A. Bonati, F. Merusi, G. Bochicchio et al., "Effect of nanoclay and conventional flame retardants on asphalt mixtures fire reaction," *Construction and Building Materials*, vol. 47, pp. 990–1000, 2013.

[9] B. Li, J. Liu, F. Han et al., "Preparation of flame retardant modified with titanate for asphalt binder," *Advances in Materials Science and Engineering*, vol. 2014, Article ID 510958, 8 pages, 2014.

[10] K. Zhu, K. Wu, B. Wu, and Z. Huang, "Investigations of the montmorillonite and aluminium trihydrate addition effects on the ignitability and thermal stability of asphalt," *Journal of Chemistry*, vol. 8, Article ID 847435, 8 pages, 2014.

[11] T. Xu and X. Huang, "A TG-FTIR investigation into smoke suppression mechanism of magnesium hydroxide in asphalt combustion process," *Journal of Analytical and Applied Pyrolysis*, vol. 87, no. 2, pp. 217–223, 2010.

[12] T. Xu and X. Huang, "Study on combustion mechanism of asphalt binder by using TG-FTIR technique," *Fuel*, vol. 89, no. 9, pp. 2185–2190, 2010.

[13] S. Bourbigot, O. Cerin, S. Duquesne, and N. Clavel, "Flame retardancy of bitumen: a calorimetry study," *Journal of Fire Sciences*, vol. 31, no. 2, pp. 112–130, 2013.

[14] F. Laoutid, M. Lorgouilloux, D. Lesueur, L. Bonnaud, and P. Dubols, "Calcium-based hydrated minerals: Promising halogen-free flame retardant and fire resistant additives for polyethylene and ethylene vinyl acetate copolymers," *Polymer Degradation and Stability*, vol. 98, no. 9, pp. 1617–1625, 2013.

[15] E. Puente, D. Lazaro, and D. Alvear, "Study of tunnel pavements behaviour in fire by using coupled cone calorimeter - FTIR analysis," *Fire Safety Journal*, vol. 81, pp. 1–7, 2016.

[16] J. Zhao, X. Huang, and T. Xu, "Combustion mechanism of asphalt binder with TG-MS technique based on components separation," *Construction and Building Materials*, vol. 80, pp. 125–131, 2015.

[17] A. Bonati, G. Bochicchio, F. Merusi et al., "Fire behaviour and beat release properties of asphalt mixtures," *International Journal of Pavement Research and Technology*, vol. 6, no. 2, pp. 100–108, 2013.

[18] T. R. Hull, A. Witkowski, and L. Hollingbery, "Fire retardant action of mineral fillers," *Polymer Degradation and Stability*, vol. 96, no. 8, pp. 1462–1469, 2011.

[19] H. Lu, J. Li, and J. Wang, "Determination of the content of sulfur of coal by the infrared absorption method with high acccuracy," *Spectroscopy and Spectral Analysis*, vol. 34, no. 2, pp. 370–375, 2014.

[20] Y. Zhong, B. Sun, B. Yang, and T. Wang, "Study of air classifier for tangentially fired boiler NOx formation characteristics in spatial distribution," *Proceedings of the CSEE*, vol. 34, no. 14, pp. 2235–2242, 2014.

[21] T. Xu, H. Shi, H. Wang, and X. Huang, "Dynamic evolution of emitted volatiles from thermal decomposed bituminous materials," *Construction and Building Materials*, vol. 64, pp. 47–53, 2014.